ACS Catalysis

Research Article

pubs.acs.org/acscatalysis

Highly-Dispersed Metallic Ru Nanoparticles Sputtered on H-Beta Zeolite for Directly Converting Syngas to Middle Isoparaffins

Jian Sun,[†] Xingang Li,[‡] Akira Taguchi,[§] Takayuki Abe,[§] Wenqi Niu,[†] Peng Lu,[†] Yoshiharu Yoneyama,[†] and Noritatsu Tsubaki*,[†]

[†]Department of Applied Chemistry, School of Engineering, [§]Hydrogen Isotope Research Center, University of Toyama, Gofuku 3190, Toyama 930-8555, Japan

[‡]Tianjin Key Laboratory of Applied Catalysis Science & Technology, School of Chemical Engineering & Technology, Tianjin University, The Collaborative Innovation Center of Chemistry and Chemical Engineering of Tianjin, Tianjin, 300072, People's Republic of China

Supporting Information

ABSTRACT: For coping with the increasing petroleum crisis, an efficient conversion of syngas (CO + H_2) to gasoline-ranged isoparafins has been paid more and more attention. Here, we report a metallic bifunctional catalyst for this conversion, consisting of highly dispersed Ru nanoparticles (NPs) and H-Beta zeolite support, prepared by a self-made polygonal barrel-sputtering process. The HRTEM and chemisorption results indicated that sputterd Ru NPs exhibited a high metal dispersion of 31.2% with a narrow diameter of 2−4 nm. These metallic Ru NPs were bonded with the acidic zeolite by a weakly physical force, clearly different from the conventional impregnated one. Without any reduction pretreatment, the Ru/H-Beta catalyst could be directly used in Fischer−Tropsch synthesis, showing a CO conversion of 1.6 times as much as the impregnated one. Furthermore, the short distance between sputtered Ru and acidic sites nearby was responsible for the enhanced C_{iso}/C_n ratio of 4.6, the highest value of gasoline-ranged hydrocarbons among the relevant reports.

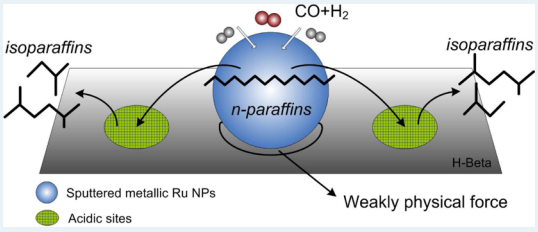

KEYWORDS: *Fischer−Tropsch synthesis, ruthenium, sputter, isoparaffin, syngas*

1. INTRODUCTION

Converting syngas (a mixture of CO and H_2) into synthetic hydrocarbons is of great importance for the increasing and sustainable development of the economy and society. The past several decades have witnessed remarkable progress in Fischer−Tropsch synthesis (FTS) to convert syngas into synthetic oil.[1−4] To date, much attention in the literature and industrial applications has been focused primarily on investigating the variety of Fe-based catalysts for olefins and Co-based catalysts for diesels. Despite its expensive cost, the ruthenium catalyst is appropriate for fundamental research owing to its higher FTS activity, chain growth probability, and attractive stability under higher partial pressures of steam or other oxygenated atmospheres compared with conventional Fe and Co catalysts.[5−9]

Concerning the selective production of C_5−C_{11} hydrocarbons, especially desirable isoparafins as synthetic gasoline, a rational strategy is to combine the FTS catalyst with an acidic zeolite via a physical mix or direct impregnation route.[10−12] However, the impregnated FTS metal onto zeolite is difficult to reduce. A physical mixture yielded very poor isoparafin selectivity. Moreover, the FTS active sites on these conventional catalysts are randomly distributed on their surface. In consideration of a consecutive reaction from syngas to isoparafins, involving production of linear hydrocarbons by FTS, hydrocracking, and isomerization, it is difficult for products desorbed on the poorly dispersed FTS sites to reach adjacent acid sites.[13] Therefore, a low efficiency for further converting linear hydrocarbons to the needed products of anti-ASF (Anderson−Schulz−Flory) law was observed. Moreover, the active metals were usually bonded with an acidic zeolite support by a strong metal support interaction (SMSI), which resulted in an incomplete reduction at a common temperature.[14−16] There is no doubt that a great challenge still remains in this filed.

From the viewpoint of support evolution, Kapteijn and coworkers recently reported that introducing mesopores in H-ZSM5 through desilication provides it with sufficient mesopore surface area to be used as an FTS catalyst support, which can clearly promote the yield toward C_{5-11} as well as the FTS activity.[17−19] For the enhanced active metals, the self-made, polygonal, barrel-sputtering process with an argon plasma stream is a powerful approach for directly depositing highly dispersed metal atoms onto powder supports, as reported by the recent literature.[20,21] In this method, the sputtered metal atoms were distributed on the support uniformly using

Received: July 17, 2013
Revised: November 3, 2013
Published: November 18, 2013

 © 2013 American Chemical Society dx.doi.org/10.1021/cs4008842 | ACS Catal. 2014, 4, 1−8

continuous hexagonal rotation and mechanical vibration. Further, this "dry" method, different from the conventional wet impregnation method, produces no wastewater containing the NO_3^- ion, which is troublesome for the environment.[22]

In present work, we have developed this self-made sputtering method on the preparation of a bifunctional Ru/H-Beta catalyst for one-step synthesis of isoparafins in the gasoline range from syngas. Sputtered metallic Ru nanoparticles on an acidic H-Beta support without any reduction could be directly used in the FTS reaction. Highly dispersed Ru sites on acidic zeolite led to intimate contact between these two catalysts, which clearly improved the consecutive reaction efficiency, including a FTS reaction and isomerization process. The sputtered bifunctional nanocatalyst achieved much higher FTS activity and more isomerization product than the conventional impregnated one.

2. EXPERIMENTAL SECTION

2.1. Catalyst Preparation. The H-Beta support was pretreated by annealing commercial HSZ-930NHA powders (NH_4^+-Beta zeolite, SiO_2/Al_2O_3 = 27 (molar), Tosoh Co.) at 550 °C for 3 h in air. A metallic ruthenium plate (99.9%, 50 × 100 mm^2, Toshima Ltd.) was used as a sputtering target. The sputtering apparatus is described in Scheme 1. Briefly, 3.0 g of

Scheme 1. Schematic Representation of the Sputtering Apparatus

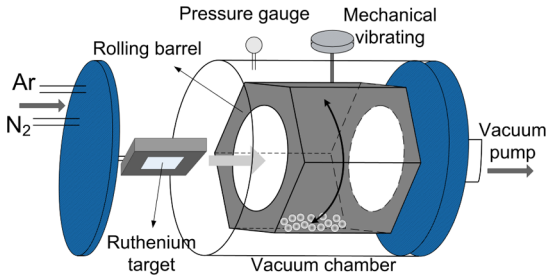

the H-Beta powders was loaded into the cavity barrel. Afterward, the vacuum chamber was evacuated to 9.9 × 10^{-4} Pa, followed by introducing pure Ar (purity: 99.995%) at a flow rate of 13 mL·min^{-1} into the chamber until the pressure reached 2.0 Pa. The input power was 200 W. After 60 min of sputtering, around 2 wt % of Ru (detected by the X-ray fluorescence spectrometry) was deposited onto the H-Beta powder. Finally, a pure N_2 flow was gradually introduced into the cavity barrel to reach room pressure and kept for 0.5 h to stabilize the metallic Ru-supported catalyst, denoted as Ru/HB-S.

For comparison, another catalyst, denoted as Ru/HB-I, with the same Ru loading was prepared through a conventional incipient wetness impregnation method. $Ru(NO_3)_3$ solution (metal concentration: 100 g·L^{-1}, Tanaka Noble Metal Co.) was impregnated onto 3.0 g of precalcined H-Beta powders, followed by aging for 12 h. The precursor was dried at 80 °C under vacuum and calcined at 400 °C for 2 h. Finally, the catalyst was reduced at 300 °C for 2 h with pure H_2 prior to the FTS reaction and is denoted as Ru/HB-I-R. For a nonzeolite support reference, a mesoporous Al_2O_3 sphere support (JRC-ALO-6, 0.35−0.83 mm, JGC Universal Ltd.), denoted as Ru/Al_2O_3-S, was used as another sputtered support under the same sputtered conditions.

2.2. Catalyst characterization. A FEI Tecnai G220 S-Twin high-resolution transmission electron microscope (HRTEM) with an accelerating voltage of 200 kV was used for the metal particle size distribution and Digital Micrograph software was employed to acquire fast Fourier transform (FFT) images.

The chemical compositions of the catalysts were determined with a Philips Magix-601 wave-dispersive X-ray fluorescence spectrometry (WD-XRF).

X-ray diffraction (XRD) analysis was performed on a Rigaku RINT 2400 diffractometer with Cu Kα radiation operated at 40 kV and 20 mA.

X-ray photoelectron spectroscopy (XPS) was obtained from the Thermo Scientific ESCALAB 250Xi equipment, and XPS peak fit was performed with Avantage Data System software.

H_2 chemisorption experiments were performed with Autosorb-1 vacuum apparatus. About 50 mg of samples was placed in a quartz cell. Prior to the measurement, the samples were degassed at 300 °C and 3.0 Pa for 1 h. The impregnated catalyst was reduced in flowing H_2 at 300 °C for 10 h and evacuated at 300 °C for 1 h to desorb any H_2, followed by cooling to 100 °C. No reduction was needed for the sputtered catalyst. The chemisorption temperature was conducted at 100 °C, and the equilibration time was 30 min. Ru dispersion was calculated assuming a H/Ru adsorption stoichiometry equal to 1.

The catalyst analyzer BELCAT-B-TT (Bel Japan Inc.) was employed to perform the H_2 temperature-programmed reduction (H_2-TPR) and NH_3 temperature-programmed desorption (NH_3-TPD) experiment at a heating rate of 10 °C·min^{-1}. To determine the reduction degree of the prereduced impregnated catalyst and directly sputtered catalyst, the O_2 titration experiment was carried out at 400 °C using the catalyst analyzer BELCAT-B-TT with the assumption that the metallic Ru atoms oxidized totally to RuO_2.

The BET surface area (S_{BET}) and micropore volume of the prepared catalysts were determined by N_2 physical adsorption at −196 °C (NOVA 2200, Quantachrome).

2.3. Evaluation of FTS Performance. Details of FTS reactions and product analysis have been reported elsewhere.[23] Briefly, the catalyst was first loaded in the center of the stainless steel reactor, and the impregnated catalyst was reduced in situ at 300 °C in H_2 flow, followed by cooling to 80 °C in N_2 before exposure to syngas. The sputtered Ru catalyst was directly heated to 260 °C without reduction. When the reaction temperature was reached, a pressurized syngas (CO/H_2, molar ratio = 1:2) was introduced, and the reaction was conducted continuously for 8 h. The W/F value (g·h·mol^{-1}), which is defined as the ratio of catalyst weight to flow rate was controlled to 10 or 15. An ice trap with the solvent (*n*-octane) of 2.0 g was set between the reactor and the back pressure regulator to capture the heavy hydrocarbons in the effluent. A trap with concentrated sulfuric acid was set after the back pressure regulator to absorb the olefins, since the separation of olefins and isoparafins by the gas chromatograph column was not so satisfying.

For the gas product, the concentration of CO, CO_2, and CH_4 in the effluent from the reactor was monitored with an online GC-TCD (Shimadzu, GC-8A) equipped with an active charcoal column. The concentration of light hydrocarbons (C_{1-6}) was analyzed with an online gas chromatograph (GC/FID, Shimadzu, GC-14B) equipped with a capillary column (J&W Scientific GS-Alumina, i.d. 0.53 mm, length = 30 m) for separating the iso and n paraffins. During online hydrocarbon analysis by GC/FID, the effluent flow rate was recorded, and

dx.doi.org/10.1021/cs4008842 | ACS Catal. 2014, 4, 1−8

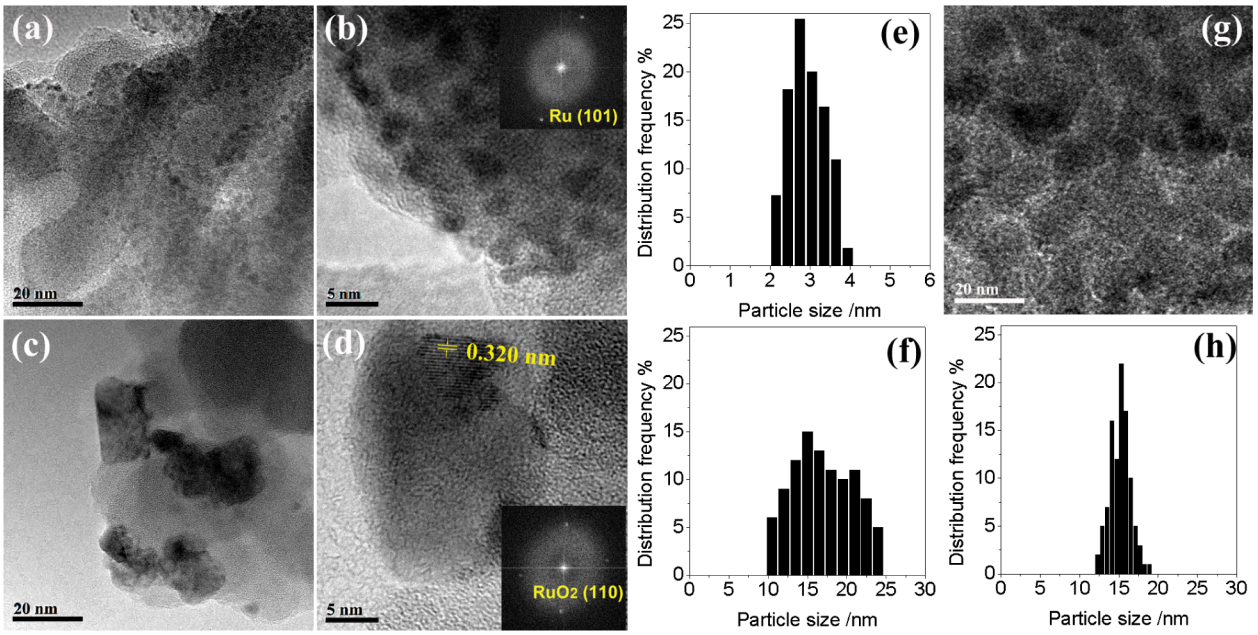

Figure 1. HRTEM images and particle size distributions (PSD) of the Ru/HB-S (a,b,e), Ru/HB-I (c,d,f), and Ru/HB-I-R(g,h) catalyst.

Table 1. Physical Structure and Chemical Characteristics of the Catalysts

catalyst	S_{BET}[a] /$m^2 \cdot g^{-1}$	micropore volume[b] /$cm^3 \cdot g^{-1}$	Ru dispersion[c] /%	d_{Ru} (chem)[d] /nm	d_{Ru} (TEM)[e] /nm
H-Beta	620.1	0.13			
Ru/HB-I-R	533.5	0.07	9.0	10.9	15.1
Ru/HB-S	579.3	0.11	31.2	3.1	2.9

[a]Determined by N_2 physical adsorption−desorption at −196 °C. [b]Obtained from the *t*-plot of N_2 physical adsorption data. [c]Determined by H_2 chemical adsorption at 100 °C. [d]Average Ru cluster size was calculated from H_2 chemisorption with $d_{Ru} = 6M/\rho\sigma N_A D$. [e]Average Ru cluster size was calculated from HRTEM statistics.

the concentration of each gaseous hydrocarbon component was determined in situ by injection of standard gas containing, for example,1% methane or 2% isobutene, etc. By this way, the formation rate of each effluent gaseous hydrocarbon component could be calculated. The yields of the olefins were obtained from the difference of the GC peaks before and after the olefins were absorbed in the H_2SO_4 trap.

For the liquid product after the reactions, the condensate hydrocarbons (C_{4+}) in the ice trap were collected, and 0.1 g of *n*-dodecane was added as the internal standard. The product was analyzed with the offline FID chromatograph (Shimadzu, GC-2014) by injection. Olefins in liquid were also obtained from the difference of the GC peaks before and after the olefins were filtered by concentrated sulfuric acid. Finally, the two results of the gas and liquid products were summed to calculate the yields of the olefins and iso and n paraffins. The FTS data for all the catalysts were collected after 6 h. The representative FTS activity was calculated by the average value from 4 to 6 h, which was the stable stage during FTS reactions.

3. RESULTS AND DISCUSSION

3.1. Metal Dispersion. Figure 1 provides a HRTEM comparison over the sputtered and conventional impregnated catalysts. Notably, the sputtered metal particles maintained a uniform spatial interval and were highly distributed on the H-Beta support with a diameter in the 2−4 nm range, owing to a continuous hexagonal rotation and mechanical vibration during Ru sputtering, which was similar to the previous report.[21] The mean particle size was calculated to be around 2.9 nm. The fast Fourier transforms (FFT) insert image in Figure 1b showed diffraction spots with a *d* spacing of 0.206 nm, corresponding to the Ru(101) lattice plane. This result implied that the sputtered Ru/HB-S catalyst consisted of metallic Ru NPs without any reduction, whereas for the impregnated one, the deposited metal clusters were aggregated and randomly dispersed on the support. The corresponding particle size distribution (PSD) revealed a wide particle size distribution ranging from 10 to 25 nm. The lattice fringe image and FFT result exhibited a typical RuO_2(110) phase with a *d* spacing of ∼0.320 nm, suggesting ruthenium oxide was the main species existing in the impregnated catalyst before regular reduction. After reduction, the impregnated catalyst exhibited a centered particle size ranging from 12 to 19 nm, with an average particle size of 15.1 nm.

As for the case of texturing information obtained by the N_2 physical adsorption−desorption test, both of the two catalysts after ruthenium loading revealed a decreased trend in the surface area compared with the raw H-Beta support. However, the sputtered one still displayed a better ability to preserve the original porosity, as reflected by the values in Table 1. Compared with H-Beta support, the losses of micropore volume were observed over both zeolite-supported catalysts. The impregnated catalyst showed fewer micropores left than the sputtered one, suggesting severe blockage of micropores during wet impregnation. The impregnated Ru solutions could easily access the internal pores, whereas the sputtered Ru was probably concentrated on the surface layer of zeolite. This trend was in accordance with the alternation of S_{BET}.

dx.doi.org/10.1021/cs4008842 | ACS Catal. 2014, 4, 1−8

The dispersion of Ru was determined by a H_2 chemisorption test. The average Ru clusters size (d_{Ru}) was calculated from dispersion data according to $d_{Ru} = 6M/\rho\sigma N_A D$ (M is the ruthenium atomic weight, ρ is the ruthenium density, σ is the atomic surface area of Ru, N_A is Avogadro's number, and D is the Ru dispersion).[24] The sputtered catalyst shows a Ru dispersion of 31.2%, three times as much as the impregnated one. The corresponding Ru clusters of 3.1 nm were much smaller than the impregnated catalyst and similar to the estimated value from HRTEM, further confirming that the sputtered Ru particles are highly dispersed and in nanoscale.

3.2. Chemical State of Ru Clusters. In general, the oxidation state of ruthenium varies: Ru^{2+}, Ru^{3+}, Ru^{4+} and Ru^{8+}. Among the family of oxides above, ruthenium dioxide is regarded as the most stable species.[25] Figure 2 compares XRD

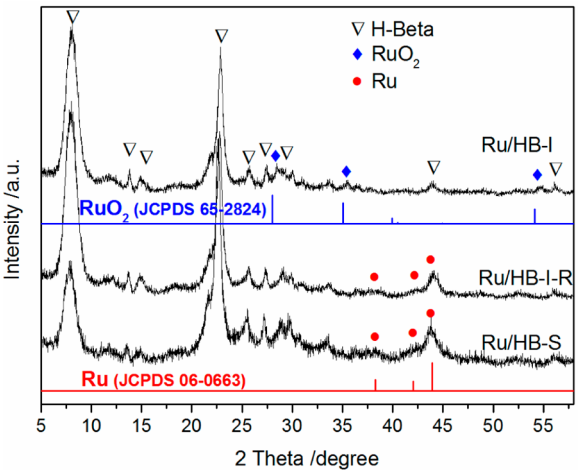

Figure 2. XRD patterns of the prepared catalysts.

patterns of the sputtered and impregnated catalysts. The Ru/HB-I catalyst reveals diffraction peaks at $2\theta = 27.9°$ and 34.9°, corresponding to (110) and (101) planes of the RuO_2 phase (JCPDS No. 65-2824). After reduction at 300 °C, pure Ru^0 phase (JCPDS No. 06-0663) appeared instead of ruthenium dioxide, whereas for the case of the Ru/HB-S catalyst, only pure and broadening metal Ru phase (obviously at $2\theta = 44.0°$) was detected, except for the H-Beta diffraction peaks, indicating that the sputtered catalyst was mainly composed of Ru^0 NPs without reduction.

H_2-TPR profiles of prepared catalysts were depicted in Figure 3. In most cases, a conventional Ru-based catalyst needs an extra reduction under 150−300 °C prior to the FTS reaction. The H_2 consumption peak at ∼177 °C on the impregnated catalyst demonstrated typical reduction behavior from ruthenium oxide to metal Ru,[26] whereas another broad and weak band from ∼650 to 820 °C (labeled with a dash box in Figure 3) was most likely to be associated with the strong metal support interaction (SMSI) between few Ru clusters and the acidic H-Beta support. The portion of Ru clusters was difficult to reduce at a common reduction temperature, as verified in the TPR curve of Ru/HB-I-R. Estimated using the TPR peak area, the ratio of unreduced to the total Ru species was ∼18.3%. This estimation of reduction degree from TPR was close to the values determined by O_2 titration method, in which the impregnated catalyst showed a reduction degree of 76.9%. Because of its low amount of unreduced Ru species, no diffraction peak of Ru oxide was observed in the Ru/HB-I-R

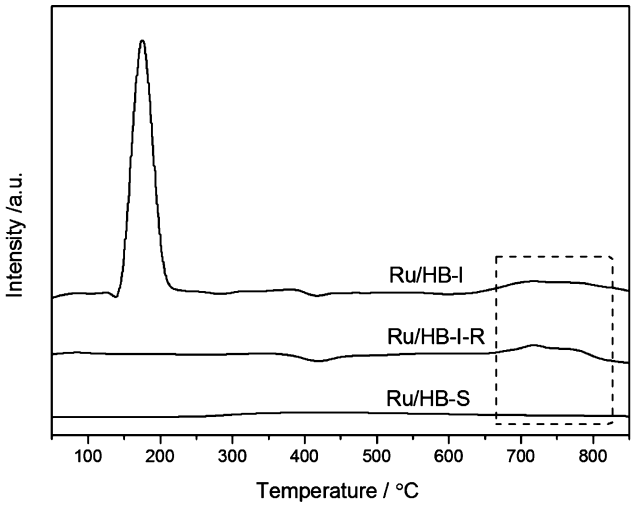

Figure 3. H_2-TPR profiles of the prepared catalysts.

XRD profile. The problem of the incomplete reduction was well solved on the sputtered Ru catalyst. No obvious peaks were observed on the Ru/HB-S curve, and the reduction degree from the O_2 titration measurement reached 92.3%, suggesting that the Ru NPs without reduction existed mainly in the form of the metallic state.

To further define the information of the Ru state, Ru 3d and Al 2p spectra of XPS tests were conducted and are shown in Figure 4. The spin−orbit coupling generally gives rise to a separation of 4.05−4.20 eV between Ru 3d 3/2 and 5/2 levels, as previously reported.[25,27] All three profiles were fitted with a Gaussian−Lorentz fitting. The Ru 3d 5/2 binding energy (BE) at 282.3, 280.7, and 279.3 eV, corresponding to 286.4, 284.8, and 283.5 eV in Ru 3d 3/2, was generally assigned to Ru(II), Ru(IV), and Ru(0) species, respectively.[27,28] The peak near 285 eV was ascribed to C 1s binding energy. Shown in the fitted curves, the impregnated Ru consisted of mainly Ru(IV) dioxide, in accordance with XRD results. After reduction in H_2, the Ru species on the impregnated H-Beta were in various states. Further quantitative XPS data showed that the primary phase was 76.9% metallic Ru, along with a few Ru(IV) and Ru(II) oxides. The presence of Ru(II) was indicative of incomplete reduction owing to the formation of the Ru−O−Al structure. In contrast, the sputtered one was composed of mainly Ru(0), accompanied by a few portions of Ru(IV) species, resulting from surface passivation in air. The molar ratio of Ru(0)/Ru(IV) was calculated to be 92.8:7.2, indicating the vast majority of Ru was in the metallic state on the sputtered catalyst surface.

In addition, the XPS element analysis demonstrated a Ru concentration of 7.71 wt % on the Ru/HB-S catalyst, which is much higher than the value of 1.62 wt % for Ru/HB-I and the value of 2.02 wt % detected by XRF. This result implies an obvious surface enrichment of Ru by the physically sputtered method. The Ru surface enrichment further demonstrates that deposited Ru particles were probably located on the external surface of the H-Beta support. This finding was clearly different from the conventional impregnated catalyst, in which deposited metals were dispersed on both the internal and external surfaces of the support.

It is worth mentioning that in Table 2, after reduction, the surface concentration of Ru on the impregnated catalyst was clearly decreased, which was confirmed by the Ru content

dx.doi.org/10.1021/cs4008842 | ACS Catal. 2014, 4, 1−8

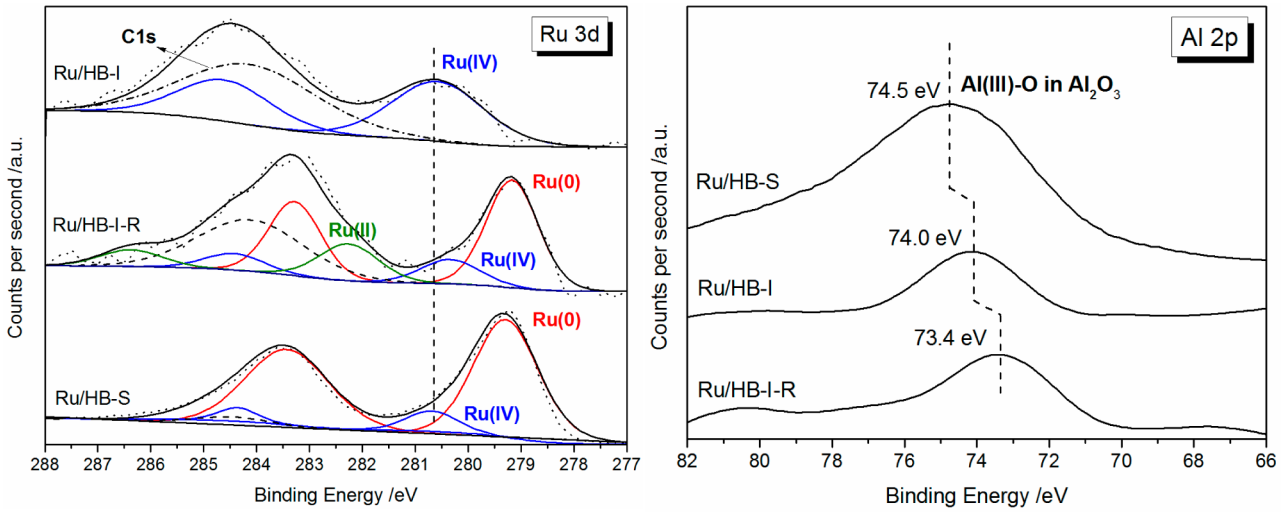

Figure 4. XPS spectra of Ru 3d and Al 2p core levels on the prepared catalysts.

Table 2. Ru Content and Chemical State in Different Catalysts

	Ru content (wt %)		Ru(n) % (XPS)		Ru(n) % (TPR)		
catalyst	XRF	XPS	Ru(0)	Ru(n^+)	Ru(0)	Ru(n^+)	Ru/O (molar)
Ru/HB-I	2.09	1.62	0	100	0	100	0.0044
Ru/HB-I-R	2.07	1.01	76.9	23.1	81.7	18.3	0.0021
Ru/HB-S	2.02	7.71	92.8	7.2	>99		0.0256

(from 1.62 to 1.01 wt %), and the molar Ru/O ratio (from 0.0044 to 0.0021). One reasonable explanation could lie in the enhanced coverage of zeolite over part of the Ru clusters, arising from the SMSI during H_2 reduction.[14,29]

For the Al 2p XPS spectra of sputtered Ru/HB-S catalyst, the binding energy peak at 74.5 eV was attributed to the Al−O bond in the H-Beta zeolite. Compared with the standard XPS handbooks, the BE value above is the same as that of the Al−O bond in bare Al_2O_3;[30] however, for the impregnated one, the corresponding peak shifted to a lower position at 74.0 eV. After reduction, this peak was further decreased to 73.4 eV, suggesting a weakening energy of the Al−O bond due to the formation of Al−O−Ru linkages, which was very consistent with the Ru 3d result. The formed interaction would reduce the chemisorptions of CO and H_2 on the surface and subsequently hinder the activation of surface reactants in FTS. In contrast, the sputtered Ru atoms were anchored on the zeolite, forming a weak physical force with the support without changing the electron structure of the H-Beta support. The metallic Ru NPs on surface play a more crucial role in activating CO and H_2 molecules at the beginning of the FTS reaction than does the conventional impregnated catalyst suffering from a SMSI.

3.3. Acidic Sites Distribution. To investigate residual acidity on the H-Beta support after two different types of Ru introduction, an NH_3-TPD experiment was conducted; the results are shown in Figure 5. The NH_3 desorption at a low temperature of 120−230 °C was associated with the weakly held NH_3 molecules, and that at a high temperature of about 250−500 °C was related to the strong Brønsted acidic sites.[31] After Ru loading, the strong acidic centers on both supported catalysts shifted to a low temperature position, indicating a weakening of acidic strength. Details of quantitative NH_3-TPD data, such as total NH_3 uptakes and amounts of acid sites of different strengths, are provided in Table S1 (Supporting Information). From the quantitative data, the two catalysts

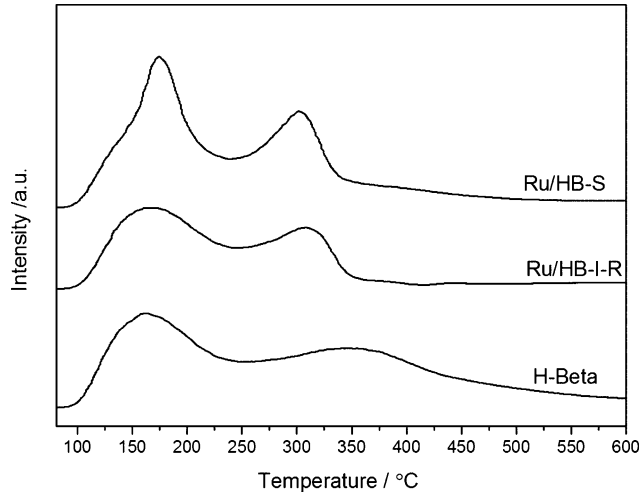

Figure 5. NH_3-TPD profiles of the Ru/HB-S, Ru/HB-I-R, and H-Beta.

showed similar weak acidic amounts, but different strong acidic amounts and total NH_3 uptakes. The calculated NH_3 uptake amount further revealed a decrease in the strong acidic amount to a different degree on the two catalysts, owing to the coverage of Ru sites after loading, as compared with the H-Beta zeolite. The sputtered catalyst reserved an ~90% strong acidic amount of H-Beta, whereas the value for the impregnated catalyst was only 57%. Clearly, the introduction of Ru from a sputtering route maintained more acidic sites at the middle strength, which would be responsible for a high isoparafin selectivity compared with the conventional impregnated route. The different interactions between deposited Ru NPs and the Al species on the acidic H-Beta were responsible for this result. The weak physical force in the sputtered catalyst could expose more Al sites on the support, which was responsible for the

dx.doi.org/10.1021/cs4008842 | ACS Catal. 2014, 4, 1−8

Table 3. FTS Performance of Different Prepared Catalysts

		selectivity /(C mol) %					
catalyst	CO conversion[a] %	CH_4	C_2-C_4	C_5-C_{11}	$C_{12}+$	C_{iso}/C_n[b]	C_{ole}/C_n[c]
Ru/HB-I-R	49.1	11.3	16.6	68.4	3.7	3.6	0.4
	78.7[d]	13.0	17.7	65.7	3.6	2.8	0.4
Ru/HB-S	78.8	10.7	17.4	71.7	0.3	4.6	0.2
Ru/Al_2O_3-S	62.3	8.9	15.1	66.8	9.2	0.3	0.5

[a]Obtained by the stable status. Reaction conditions: 260 °C, 1.0 MPa, and W/F = 10 g·h·mol^{-1}. [b]C_{iso}/C_n is the molar ratio of all isoparafins to all normal paraffins with $n > 3$. [c]C_{ole}/C_n is the molar ratio of olefin to all normal paraffins with $n > 1$. [d]Obtained at a W/F value of 15 g·h·mol^{-1}.

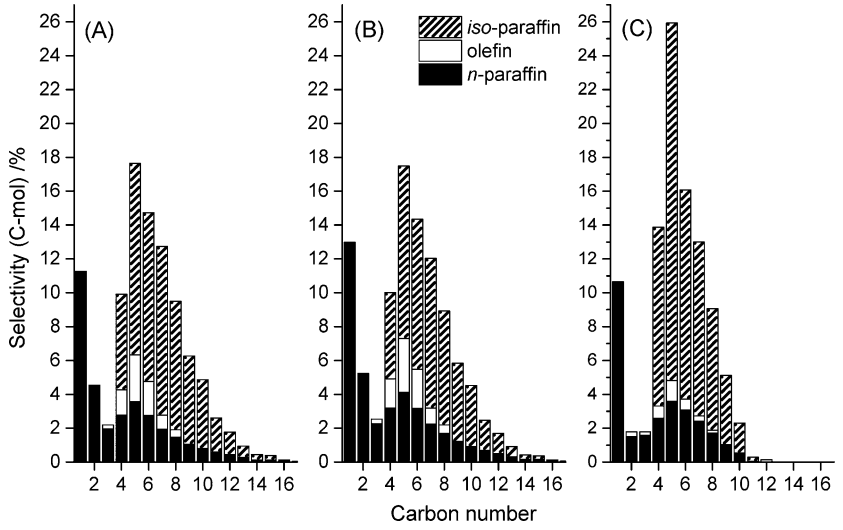

Figure 6. FTS product distribution of the Ru/HB-I-R (W/F = 10) (A), Ru/HB-I-R (W/F = 15) (B), and Ru/HB-S (W/F = 10) (C).

acidic sites; however, the strong interaction from the reduction of Ru/HB-I promoted the formation of an Al−O−Ru structure, and thus, a large number of acidic sites from the Al species were covered.

3.4. Direct Isoparaffin Synthesis via FTS Performance. FTS results and a detailed product distribution of the different prepared catalysts are listed in Table 3 and Figure 6. Abe and co-workers have reported the sputtered Ru nanoparticles on the TiO_2 support were much more active than the conventional catalyst in the field of CO_2 methanation.[21] Herein, a similar performance comparison was observed in the bifunctioanl FTS catalyst. Apparently, the sputtered Ru/H-Beta catalyst performed a CO conversion 1.6 times as great as the impregnated catalyst under the same FTS condition. The space velocity of the Ru/HB-I-R catalyst was lowered to obtain an isoconversion level (∼79%) to Ru/HB-S. Clearly, at an isoconversion level, the C_{iso}/C_n ratio of impregnated catalyst was decreased to 2.8, much lower than that of sputtered one and that at a high space velocity. The CH_4 and C_{12+} selectivity of the sputtered catalyst was less, but C_{5-11} hydrocarbons were more abundant than those of the impregnated catallyst. Moreover, the isoparafin selectivity was enhanced with a hydrocarbon distribution centered at a carbon number of 4−10. To the best of our knowledge, the obtained C_{iso}/C_n ratio of 4.6 is the highest value of gasoline-range hydrocarbons among relevant FTS reports.[13,32,33] On the basis of the characterization results, the highly dispersed Ru NPs and weak interaction between deposited Ru and H-Beta should be responsible for this result.

To obtain the accurate turnover frequency (TOF) value, we adjusted the space velocity of the FTS reaction for a lower CO conversion level (∼10%). The calculated TOF value was 0.129 s^{-1} for the Ru/HB-S catalyst at a CO conversion of 10.6%, and 0.267 s^{-1} for the Ru/HB-I catalyst at a CO conversion of 9.5%. Clearly, the TOF value of the impregnated catalyst was higher than that of the sputtered catalyst. This result was correlated to the different Ru particle size,[34,35] but the TOF value was not the only conclusive reason for catalytic activity. As supported by the HRTEM and XPS results, the high catalytic activity of the Ru/HB-S catalyst should be attributed mainly to its much higher number of effective surface active sites than that of Ru/HB-I.

Scheme 2 provided a possible one-step synthesis process of isoparafins from syngas on the sputtered metallic Ru NPs. Liner hydrocarbons (n paraffins) were first produced from the chain growth reaction in FTS. By means of the highly dispersed Ru NPs as FTS active centers, the obtained long-chain hydrocarbons possessed a greater opportunity than the poorly dispersed impregnated catalyst to reach neighboring acidic sites

Scheme 2. One-Step Synthesis of Isoparafins from Syngas on the Sputtered Metallic Ru NPs

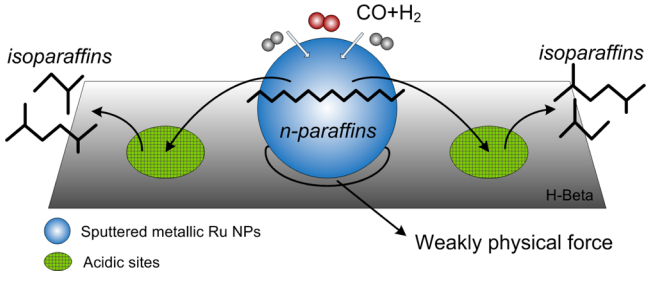

dx.doi.org/10.1021/cs4008842 | ACS Catal. 2014, 4, 1−8

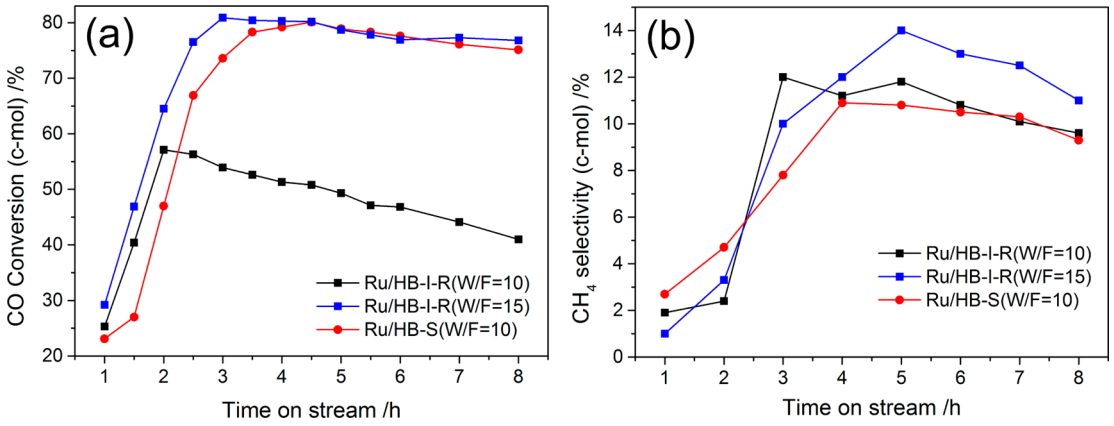

Figure 7. Time-on-stream (TOS) evolution of CO conversion (a) and CH_4 selectivity (b) during FTS reactions.

on the H-Beta support, where linear hydrocarbons were hydrocracked and isomerized to generate isoparafin products centered at C_4–C_{11}. An additional ASF plot and the α value comparison of two prepared catalysts at an isoconversion level are given Figure S1 (Supporting Information). Carbon chain growth probability in FTS could be reflected by the ASF plot and α value. It was inferred from the lower α values that the production of long chains was suppressed as a result of acidic catalysis on both zeolite-supported Ru catalysts. Relatively, the sputtered catalyst exhibited an α value of 0.67, lower than the 0.72 for the impregnated one. Such suppression of heavy-hydrocarbon production was conducted more intensely on the sputtered catalyst, which resulted from the shorter distance between the highly dispersed Ru and acidic sites.

Moreover, the weak physical force between the Ru NPs and the H-Beta support made it facile to activate the surface-adsorbed CO and H_2 molecules. It is reported that sputtered metal nanoparticles for the FTS are able to adsorb and activate more CO molecules on the surface as compared with the larger impregnated particles.[36] The more exposed metallic Ru^0 sites in the sputtered catalyst achieved a more facile activation process than in the impregnated one, and as a result, the CO conversion was strikingly accelerated on the sputtered catalyst. Therefore, a high FTS activity and more of the expected isomerization product for a consecutive multireaction on one nanocatalyst were achieved successfully.

For other nonzeolite support, the physically sputtered method is also effective in depositing noble metals. A commercial mesoporous Al_2O_3 (JRC-ALO-6) was applied as a support to compare its catalytic activity with the Ru/HB-S catalyst. The FTS activity for the Ru/Al_2O_3-S reached a competitive value of 62.3% under the same conditions as the zeolite-supported catalyst. Different from the bifunctional Ru/HB-S catalyst, the carbon chain growth reaction was the primary step when there were not enough acidic sites; therefore, the isoparafin selectivity over the Al_2O_3 support was much lower than the bifunctional one. In addition, the selectivity of long-chain hydrocarbons (C_{12+}) increased from 0.3 to 9.2, further indicating that hydrocracking of a heavy product was enhanced on the acidic H-Beta support.

3.5. Stabilities of Prepared Catalysts during FTS Reactions. The time-on-stream (TOS) evolutions of CO conversion and CH_4 selectivity over Ru/HB-S and Ru/HB-I-R catalysts are provided in Figure 7. For the three reactions, the observed stability order was as follows: Ru/HB-I-R (W/F = 15) > Ru/HB-S (W/F = 10) > Ru/HB-I-R (W/F = 10). Specifically, under the same FTS conditions (W/F = 10), the impregnated catalyst showed a faster decrease in CO conversion after 8 h than the sputtered catalyst. After the space velocity decreased (W/F = 15) for the impregnated catalyst, the stability was clearly promoted. At an isoconversion level, the two catalysts exhibited almost the same conversion at the TOS of 4–6 h, followed by a slight decrease in the catalytic activity. Compared with the last 2 h after the isoconversion time in the reaction, the loss of activity on the sputtered catalyst (6.2%) was slightly greater than that of the impregnated catalyst (5.1%). The lifetime results demonstrated that the sputtered Ru clusters bounded by the zeolite with a weak physical force were reliable and comparable to the conventional catalyst.

For the evolution of product selectivities, CH_4 selectivity was simultaneously increased, with the CO conversion increasing at the initial 2 or 3 h, indicating the start-up stage of the FTS process. It became stable and gradually decreased after 3 h, which was in agreement with the CO conversion evolution. Compositions of light hydrocarbons (C_{1-3}) at start-up and level-off stages are compared in Figure S3 (Supporting Information). It is important to point out that the ratios of light olefins, including ethylene and propylene in C_{1-3} hydrocarbons, were less at the level-off stage than at the start-up stage for both catalysts. It is noted that different from the fresh catalyst surface at the start-up stage, the catalyst surface at the level-off stage was covered partly by some waxy hydrocarbons, where the waxy hydrocarbon layer hindered the diffusion of the produced FTS hydrocarbons and allowed the 1-olefins, such as ethylene and propylene, to be readsorbed more readily and, finally, hydrogenated on Ru.

To investigate possible sintering for the two catalysts, additional TEM pictures of Ru/HB-S and Ru/HB-I-R after FTS reactions under the same conditions are provided in Figure S2 (Supporting Information). It was observed that both catalysts after FTS reaction showed a particle size increase if compared with the catalysts before reaction. The average particle size of the sputtered catalyst increased from 2.9 to 4.9 nm, accompanied by the growth of a few Ru NPs. This result was attributed to the weak physical interaction between the Ru NPs and the support. The impregnated Ru particles after FTS increased to 18.7 nm, a clear growth of 3.6 nm. It appeared that part of the Ru clusters of this catalyst trended to aggregation and sintering. The migration of Ru clusters produced the decreased surface active sites. That is the reason why the time-on-stream activity over the sputtered catalyst was more stable

dx.doi.org/10.1021/cs4008842 | ACS Catal. 2014, 4, 1–8

than over the impregnated catalyst under the same FTS conditions.

4. CONCLUSIONS

A physically sputtered Ru/H-Beta bifunctional catalyst was successfully prepared via a self-made polygonal barrel-sputtering device. The synthesized catalyst could be directly employed for the FTS reaction without any heat treatment and H_2 reduction. Highly dispersed metallic Ru NPs and a weak interaction with the H-Beta support were responsible for the clearly promoted FTS activity. Meanwhile, the optimized acidic distribution by the sputtering procedure resulted in the production of more middle isoparafins than the conventional impregnated method. The physical sputtering process provided a new strategy in solving the SMSI problem arising from the conventional impregnated route and subsequently promoted yield of product in the gasoline ranged.

■ ASSOCIATED CONTENT

Supporting Information

ASF plot comparison, TEM and PSD images after FTS reactions, composition of light hydrocarbons at start-up and level-off stages during FTS, quantitative NH_3-TPD data. This material is available free of charge via the Internet at http://pubs.acs.org.

■ AUTHOR INFORMATION

Corresponding Author

*Phone: +(81)-76-445-6846. Fax: +(81)-76-445-6846. E-mail: tsubaki@eng.u-toyama.ac.jp.

Notes

The authors declare no competing financial interest.

■ ACKNOWLEDGMENTS

This work was financially supported by the National Natural Science Foundation of China (U1162103).

■ REFERENCES

(1) Shafer, W. D.; Jacobs, G.; Davis, B. H. *ACS Catal.* **2012**, *2*, 1452−1456.
(2) Kang, J.; Zhang, S.; Zhang, Q.; Wang, Y. *Angew. Chem., Int. Ed.* **2009**, *48*, 2565−2568.
(3) Chen, W.; Fan, Z.; Pan, X.; Bao, X. *J. Am. Chem. Soc.* **2008**, *130*, 9414−9419.
(4) Sun, J.; Xing, C.; Xu, H.; Meng, F.; Yoneyama, Y.; Tsubaki, N. *J. Mater. Chem. A* **2013**, *1*, 5670−5678.
(5) Kang, J.; Cheng, K.; Zhang, L.; Zhang, Q.; Ding, J.; Hua, W.; Lou, Y.; Zhai, Q.; Wang, Y. *Angew. Chem., Int. Ed.* **2011**, *50*, 5200−5203.
(6) Simonetti, D. A.; Rass-Hansen, J.; Kunkes, E. L.; Soares, R. R.; Dumesic, J. A. *Green Chem.* **2007**, *9*, 1073−1083.
(7) Xiao, C. X.; Cai, Z. P.; Wang, T.; Kou, Y.; Yan, N. *Angew. Chem., Int. Ed.* **2008**, *47*, 746−749.
(8) Li, C.; Xu, H.; Kido, Y.; Yoneyama, Y.; Suehiro, Y.; Tsubaki, N. *ChemSusChem* **2012**, *5*, 862−866.
(9) Shi, L.; Tao, K.; Kawabata, T.; Shimamura, T.; Zhang, X. J.; Tsubaki, N. *ACS Catal.* **2011**, *1*, 1225−1233.
(10) Tsubaki, N.; Yoneyama, Y.; Michiki, K.; Fujimoto, K. *Catal. Commun.* **2003**, *4*, 108−111.
(11) Yoneyama, Y.; He, J.; Morii, Y.; Azuma, S.; Tsubaki, N. *Catal. Today* **2005**, *104*, 37−40.
(12) Xiong, H.; Zhang, Y.; Wang, S.; Liew, K.; Li, J. *J. Phys. Chem. C* **2008**, *112*, 9706−9709.
(13) Bao, J.; He, J.; Zhang, Y.; Yoneyama, Y.; Tsubaki, N. *Angew. Chem., Int. Ed.* **2008**, *47*, 353−356.
(14) de la Pena O'Shea, V. A.; Consuelo Alvarez Galvan, M.; Platero Prats, A. E.; Campos-Martin, J. M.; Fierro, J. L. G. *Chem. Commun.* **2011**, *47*, 7131−7133.
(15) Liu, X.; Liu, M.-H.; Luo, Y.-C.; Mou, C.-Y.; Lin, S. D.; Cheng, H.; Chen, J.-M.; Lee, J.-F.; Lin, T.-S. *J. Am. Chem. Soc.* **2012**, *134*, 10251−10258.
(16) Farmer, J. A.; Campbell, C. T. *Science* **2010**, *329*, 933−936.
(17) Sartipi, S.; Parashar, K.; Makkee, M.; Gascon, J.; Kapteijn, F. *Catal. Sci. Technol.* **2013**, *3*, 572−575.
(18) Sartipi, S.; Parashar, K.; Valero-Romero, M. J.; Santos, V. P.; van der Linden, B.; Makkee, M.; Kapteijn, F.; Gascon, J. *J. Catal.* **2013**, *305*, 179−190.
(19) Sartipi, S.; van Dijk, J. E.; Gascon, J.; Kapteijn, F. *Appl. Catal., A* **2013**, *456*, 11−22.
(20) Honda, Y.; Akamaru, S.; Inoue, M.; Abe, T. *Chem. Eng. J.* **2012**, *209*, 616−622.
(21) Abe, T.; Tanizawa, M.; Watanabe, K.; Taguchi, A. *Energy Environ. Sci.* **2009**, *2*, 315−321.
(22) Zeng, C.; Sun, J.; Yang, G.; Ooki, I.; Hayashi, K.; Yoneyama, Y.; Taguchi, A.; Abe, T.; Tsubaki, N. *Fuel* **2013**, *112*, 140−144.
(23) He, J.; Liu, Z.; Yoneyama, Y.; Nishiyama, N.; Tsubaki, N. *Chem.—Eur. J.* **2006**, *12*, 8296−8304.
(24) Carballo, J. M. G.; Finocchio, E.; García, S.; Rojas, S.; Ojeda, M.; Fierro, J. L. G. *Catal. Sci. Technol.* **2011**, *1*, 1013−1023.
(25) Mun, C.; Ehrhardt, J. J.; Lambert, J.; Madic, C. *Appl. Surf. Sci.* **2007**, *253*, 7613−7621.
(26) Mazzieri, V.; Coloma-Pascual, F.; Arcoya, A.; L'Argentière, P.; Fıgoli, N. *Appl. Surf. Sci.* **2003**, *210*, 222−230.
(27) Elmasides, C.; Kondarides, D. I.; Grünert, W.; Verykios, X. E. *J. Phys. Chem. B* **1999**, *103*, 5227−5239.
(28) Pylypenko, S.; Blizanac, B. B.; Olson, T. S.; Konopka, D.; Atanassov, P. *ACS Appl. Mater. Interfaces* **2009**, *1*, 604−611.
(29) Liu, J. *ChemCatChem* **2011**, *3*, 934−948.
(30) Eberhardt, M. A.; Proctor, A.; Houalla, M.; Hercules, D. M. *J. Catal.* **1996**, *160*, 27−34.
(31) Cheng, K.; Kang, J.; Huang, S.; You, Z.; Zhang, Q.; Ding, J.; Hua, W.; Lou, Y.; Deng, W.; Wang, Y. *ACS Catal.* **2012**, *2*, 441−449.
(32) Li, X.; He, J.; Meng, M.; Yoneyama, Y.; Tsubaki, N. *J. Catal.* **2009**, *265*, 26−34.
(33) Li, X.; Feng, X.; Ge, Q.; Fujimoto, K. *Fuel* **2008**, *87*, 534−538.
(34) Karim, A. M.; Prasad, V.; Mpourmpakis, G.; Lonergan, W. W.; Frenkel, A. I.; Chen, J. G.; Vlachos, D. G. *J. Am. Chem. Soc.* **2009**, *131*, 12230−12239.
(35) Bezemer, G. L.; Bitter, J. H.; Kuipers, H. P. C. E.; Oosterbeek, H.; Holewijn, J. E.; Xu, X.; Kapteijn, F.; van Dillen, A. J.; de Jong, K. P. *J. Am. Chem. Soc.* **2006**, *128*, 3956−3964.
(36) Li, X.-G.; Liu, C.; Sun, J.; Xian, H.; Tan, Y.-S.; Jiang, Z.; Taguchi, A.; Inoue, M.; Yoneyama, Y.; Abe, T.; Tsubaki, N. *Sci. Rep.* **2013**, *3*, 2813.